doi:10.1016/j.jmb.2006.04.030 J. Mol. Biol. (2006) 359, 1235–1248

JMB

Available online at www.sciencedirect.com

SCIENCE DIRECT®

ELSEVIER

Following the Dynamics of Changes in Solvent Accessibility of 16 S and 23 S rRNA During Ribosomal Subunit Association Using Synchrotron-generated Hydroxyl Radicals

Thuylinh Nguyenle[1], Martin Laurberg[1] Michael Brenowitz[2]* and Harry F. Noller[1]*

[1]*Center for Molecular Biology of RNA and Department of Molecular, Cell and Developmental Biology University of California Santa Cruz, 225 Sinsheimer Laboratories, Santa Cruz CA 95064, USA*

[2]*Department of Biochemistry and Center for Synchrotron Biosciences, Albert Einstein College of Medicine, 1300 Morris Park Avenue, Bronx NY 10461, USA*

**Corresponding authors*

We have probed the structure and dynamics of ribosomal RNA in the *Escherichia coli* ribosome using equilibrium and time-resolved hydroxyl radical (·OH) RNA footprinting to explore changes in the solvent-accessible surface of the rRNA with single-nucleotide resolution. The goal of these studies is to better understand the structural transitions that accompany association of the 30 S and 50 S subunits and to build a foundation for the quantitative analysis of ribosome structural dynamics during translation. Clear portraits of the subunit interface surfaces for 16 S and 23 S rRNA were obtained by constructing difference maps between the ·OH protection maps of the free subunits and that of the associated ribosome. In addition to inter-subunit contacts consistent with the crystal structure, additional ·OH protections are evident in regions at or near the subunit interface that reflect association-induced conformational changes. Comparison of these data with the comparable difference maps of the solvent-accessible surface of the rRNA calculated for the *Thermus thermophilus* X-ray crystal structures shows extensive agreement but also distinct differences. As a prelude to time-resolved ·OH footprinting studies, the reactivity profiles obtained using Fe(II)EDTA and X-ray generated ·OH were comprehensively compared. The reactivity patterns are similar except for a small number of nucleotides that have decreased reactivity to ·OH generated from Fe(II)EDTA compared to X-rays. These nucleotides are generally close to ribosomal proteins, which can quench diffusing radicals by virtue of side-chain oxidation. Synchrotron X-ray ·OH footprinting was used to monitor the kinetics of association of the 30 S and 50 S subunits. The rates individually measured for the inter-subunit contacts are comparable within experimental error. The application of this approach to the study of ribosome dynamics during the translation cycle is discussed.

Keywords: ribosomes; subunit interface; intersubunit bridges; chemical probing; association kinetics

Introduction

The ribosome is a large and complicated ribonucleoprotein composed of two asymmetric subunits that work cooperatively to synthesize protein. X-ray crystal structures of the 70 S ribosome with its functional ligands, the isolated 30 S and 50 S subunits and cryo-electron micrographic (cryo-EM) reconstructions reveal that the functional centers of the translational machine, including the mRNA binding site, the tRNA binding sites, the decoding site, and the peptidyl transferase catalytic center, are within a cavity at the subunit interface.[1–9] The nucleotides surrounding the inter-subunit cavity are

Abbreviations used: cryo-EM, cryo-electron microscopy; DMS, dimethyl sulfate.

E-mail addresses of the corresponding authors: brenowit@aecom.yu.edu; harry@nuvolari.ucsc.edu

highly conserved among the Archaea, Bacteria and Eucarya phylogenetic domains.[10]

The subunits adhere to each other *via* inter-subunit bridges[1,8,11] several of which are in close proximity to the mRNA and tRNA binding sites (Figure 1). These bridges play a key role in translation, since the 30 S and 50 S subunits move with respect to each other[12] and must communicate to synchronize the movement of mRNA and tRNAs during different states of the translational cycle. Hydroxyl radical generated by Fe(II)EDTA-catalyzed Fenton chemistry[13] is a useful probe of the solvent accessibility of the ribosomal RNA (rRNA) in both isolated subunits and associated ribosomes.[14,15] The small, neutral and diffusible ·OH abstracts hydrogen atoms from solvent-accessible ribose sugars, largely independent of sequence and structural context, resulting in cleavage of the RNA backbone that is readily detected by gel electrophoresis. Footprinting with ·OH and base-specific probes identified an extensive list of nucleotides in the 16 S and 23 S rRNA involved in subunit–subunit interactions prior to the solution of the three-dimensional structures of the *Thermus thermophilus* 70 S ribosome.[14–20] Inter-subunit bridges were also described from cryo-EM structures of *Escherichia coli* ribosomes.[8,21,22] The 5.5 Å resolution X-ray crystal structure of the 70 S ribosome reveals more than 30 molecular contacts across 12 inter-subunit bridges.[4]

Under physiological conditions, association of the 30 S and 50 S subunits to form a functional 70 S ribosome occurs with the assistance of initiation factors and in the presence of mRNA and tRNA. However, isolated 30 S and 50 S subunits associate into vacant 70 S ribosomes autonomously. The reversible association of the ribosomal subunits shows that the subunits are in thermodynamic equilibrium:[23,24]

$$30S + 50S \underset{k_d}{\overset{k_a}{\rightleftharpoons}} 70S$$

This reaction is dependent upon multiple thermodynamic variables including the concentration of cations. At ~4 mM Mg^{2+} comparable to physiological levels, the equilibrium strongly favors association; dissociation is favored at Mg^{2+} concentrations below 2 mM.[26] The rate of subunit association is slower than diffusion limited.[25]

Here, we describe equilibrium and time-resolved quantitative ·OH footprinting studies of association of the ribosomal subunits. The goals of this work are to (i) determine in solution the ensemble of rRNA contacts that define the subunit interface of the *E. coli* ribosome and (ii) measure their time-dependent formation. Comparison of the ·OH footprinting reactivity profiles with the solvent-accessible surfaces calculated from 30 S and 50 S subunit crystal structures[2,3] and of the 70 S T. *thermophilus* ribosome crystal structure[1] reveals some features of rRNA that are protected upon association, but are not directly involved in the subunit interface, indicating the existence of association-dependent conformational changes. Time-dependent formation of the rRNA bridges during subunit assembly was followed with synchrotron X-ray ·OH footprinting.[27] Subtle differences are observed between generation of ·OH by Fe-EDTA-mediated Fenton chemistry *versus* X-ray radiolysis. These studies provide the foundation for time-

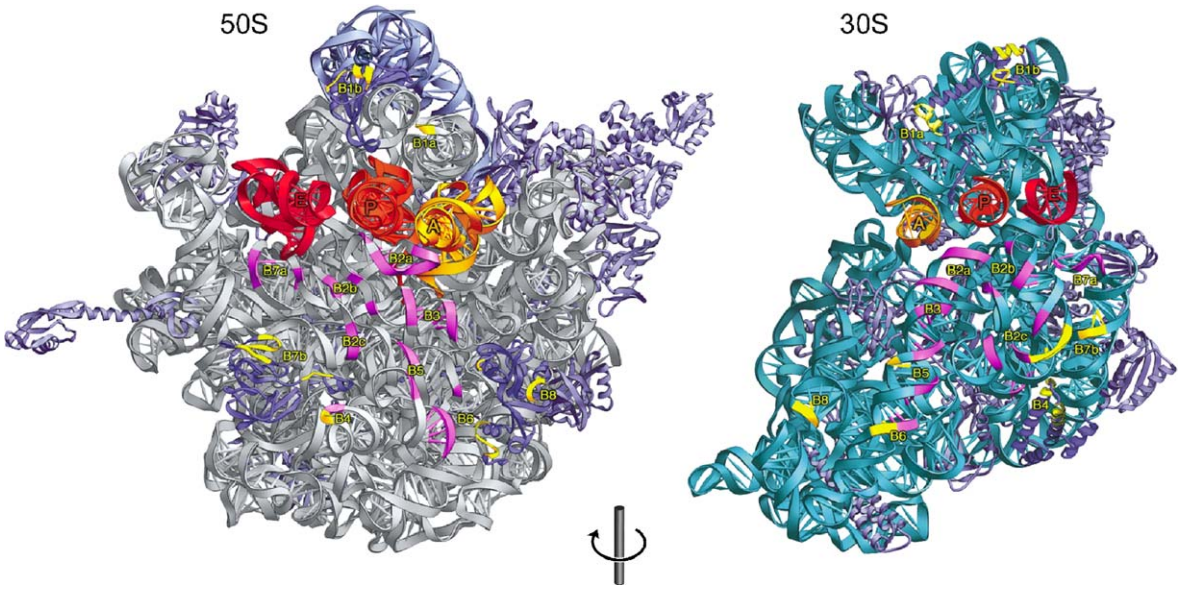

Figure 1. The interface surfaces of the 30 S and 50 S ribosomal subunits from the 5.5 Å resolution X-ray crystal structure of the *T. thermophilus* 70 S ribosome.[1] tRNA molecules bound to the A, P and E sites are shown in yellow, orange and red, respectively. The inter-subunit bridges are labeled and colored magenta (RNA–RNA contacts) or yellow (protein–RNA and protein–protein contacts). The subunits are rotated 180° with respect to each other around the vertical axis, relative to their orientations in the 70 S ribosome.

resolved studies of translational processes at single-nucleotide resolution using synchrotron X-ray-generated hydroxyl radicals.

Results

Mapping the subunit interface

The ·OH reactivity profiles of the 16 S and 23 S rRNA within the isolated 30 S and 50 S subunits, respectively, and within the assembled 70 S ribosome were quantified with single-nucleotide precision as described in Materials and Methods. To facilitate and clarify the presentation of the many thousands of results and their interpretation in a concise form, the ·OH reactivity changes that reflect subunit association are summarized by taking the ratio of reactivity in 70 S ribosomes to that of the isolated subunits (70 S/30 S and 70 S/50 S, respectively; Figure 2). This transformation normalizes the ·OH reactivity data by eliminating rescaling between electrophoretic profiles due to variations in the primer extension reactions such as those due to the distance between primer positions and target nucleotides.

The reactivity ratios were determined for ·OH generated by Fe(II)EDTA mediated Fenton chemistry (Figure 2(b)) and X-ray radiolysis (Figures 2(c) and (d)). A threshold of twice the standard deviation (2σ) was used to identify nucleotides whose reactivity changes significantly exceed the noise in the data. The reactivity ratios of only a small subset of nucleotides exceed this threshold (Figure 2). A list of the protected regions is

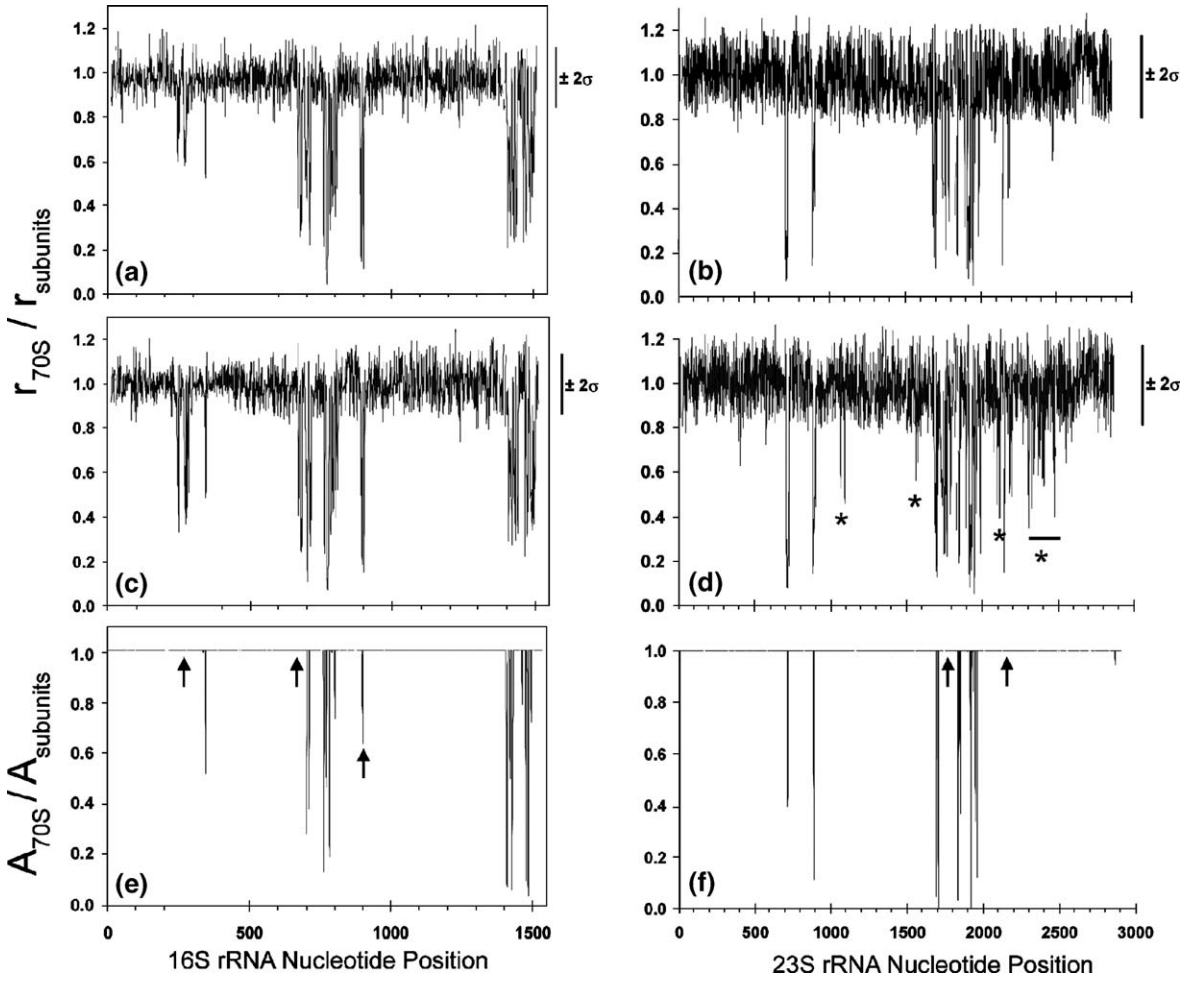

Figure 2. (a) and (d) Changes in ·OH reactivity of nucleotides in 16 S and 23 S rRNA that occur upon association of the 30 S and 50 S ribosomal subunits. Reactivity ratios (r_{70S} /$r_{subunits}$) for (a) and (c) 70 S/30 S and (b) and (d) 70 S/50 S were determined using ((a) and (b)) Fe(II)-EDTA or ((c) and (d)) synchrotron X-rays to generate the ·OH for footprinting. (e) and (f) Ratios of solvent-exposed surface areas ($A_{70S}/A_{subunits}$) in 70 S *versus* 30 S accessible to a 1.4 Å sphere for the 16 S and 23 S rRNA, respectively, calculated using the NACCESS program based on the ribosome crystal structure (see Materials and Methods). Nucleotides whose magnitudes exceed the 2σ threshold are listed in Tables 1 and 2. Asterisks in (d) indicate nucleotides protected in X-ray, but not Fe(II)-EDTA probing experiments. The arrows in (e) and (f) indicate nucleotides in the 70 S particle that are protected from ·OH in boh the X-ray or Fe-EDTA experiments that are solvent accessible by NACCESS analysis of the crystal structures.

Table 1. 16S rRNA nucleotide positions protected by subunit association

Inter-subunit bridge	·OH protection	NACCESS	Molecular contacts[a]
2a	1407–1416	1407–1410	1408–1410
	1492–1495	1494–1495	1494–1495
2b	782–785	783–785	784–785
	789–802	791	794
	–	–	1516–1519
2c	770–772	770–771	770–771
	889–902	899–900	900–901
3	1483–1490	1483–1486	1484–1486
4	760–762	762–763	763–764
5	1418–1422	1419–1421	1418–1422
5, 6	1471–1476	1474–1476	1474–1476
6	1425–1432	1427–1431	1429–1431
7a	694–704	702	698, 702
7b	709–714	712–713	712–713
	773–777	773	773–776
8	344–346	346	345–347

[a] Inter-subunit molecular contacts reported by inspection of 5.5 Å X-ray crystal structure.[1]

summarized in Tables 1 and 2. Some differences are evident between the maps obtained using Fe-EDTA or X-ray radiolysis to generate the ·OH used for footprinting. The differences observed for 16 S rRNA reflect minor changes in the extent of protection rather than the presence or absence of certain protections. In 23 S rRNA, some nucleotides are protected when X-ray radiolysis rather than Fe(II)EDTA is used to generate ·OH (Figure 2; compare the regions indicated by an asterisk in (d) with (b)). These differences around positions 1100, 1500, 2100 and 2300–2500 of the 23 S rRNA are discussed later in this section.

We next asked how the differences in solvent accessibility due to subunit association determined by ·OH mapping compare with the X-ray crystal structure of the ribosome. This comparison was accomplished by constructing an all-atom model of the 5.5 Å X-ray crystal structure of the *T. thermophilus* ribosome as described in Materials and Methods. A model for the 30 S subunit portion of the 70 S ribosome was constructed based on the homologous high-resolution structure of the *T. thermophilus* 30 S subunit,[2] while the 50 S all-atom model was constructed based on the heterologous high-resolution *Haloarcula marismortui*[3] and *Deinococcus radiodurans*[28] structures, as described in Materials and Methods. The solvent-accessible surface of the C4′ and C5′ atoms of each ribose moiety in the model was calculated using NACCESS†[29] to roll a 1.4 Å radius sphere over the van der Waals surfaces of the 70 S ribosome and the separate 30 S and 50 S subunits. The ratios of the solvent-accessible surface of each nucleotide in the 70 S ribosome to those of the isolated subunits are summarized in Figure 2(e) and (f).

† Hubbard, S.J. & Thornton, J.M. (1993). 'NACCESS', Computer Program. Department of Biochemistry and Molecular Biology, University College London.

Table 2. 23 S rRNA nucleotide positions protected by subunit association

Inter-subunit bridge	·OH protection	NACCESS	Molecular contacts[a]
1a	883–896	886–887	886–888
2a	1911–1913	1912	1913–1914
	1417–1418	–	1918
2b	–	1835–1837	1836–1837
	1919–1926	1919–1920	1919–1920
	1921–1926	–	1922
	1928, 1930–1932	1931–1932	1932
2c	1831–1835	1831–1832	1832–1833
3	1946–1952	1948–1948	1947–1948
	1959–1964	1960–1961	1960–1961
4	708–724	713–716	713, 717–718
5	1683–1688	1687–1688	1689–1690
	1765–1769	–	1768–1769
	1987–1991	–	1989
5, 6	1689–1694	1689–1690	1689–1690
6	1701–1705	1702–1704	1702–1705
7a	1844–1849	1847–1848	1848–1849
	–	–	1896

[a] Inter-subunit molecular contacts reported by inspection of 5.5 Å X-ray crystal structure.[1]

The impression provided by Figure 2 is one of overall agreement between the solvent accessibility maps calculated from ·OH footprinting and from the crystal structure, consistent with the conclusions previously drawn from inspection.[1] However, differences are evident (Figure 2(e) and (f); nucleotides marked by arrows; Table 3). The solvent-accessible surface ratios calculated from the all-atom models are derived from rigid-body approximations that do not reflect conformational changes that accompany association. Therefore, differences between the ·OH mapping and NACCESS surfaces reflect changes in the subunit structures following their assembly into a functional ribosome. An analysis comparable to those shown above for the 16 S and 23 S rRNA was also conducted for the 5 S rRNA. Since significant changes to its ·OH reactivity were not observed upon subunit association, it is not considered further.[30]

Table 3. Nucleotides of rRNA that show differences in accessibility between hydroxyl radical probing and solvent accessibility calculated from the X-ray structure using NACCESS

16 S rRNA	23 S rRNA
245–250, 269–275, 278–281, 284	403–405, 409
670–672, 679–682	1065–1067, 1094–1095
806–809	1573–1574, 1577, 1579, 1582–1586, 1589, 1591–1597
	1709–1711, 1722, 1734, 1726–1740, 1743–1752, 1754–1756
	2098–2102, 2106–2107, 2111–2126, 2144–2148, 2181–2183, 2191–2193
	2303, 2305–2310, 2325–23252339–2343, 2349, 2368–2371, 2375–2376, 2381, 2399–2410

Differences between solution probing and crystallographic calculation of solvent-accessible surface

Quantification of the solvent accessibility in solution by ·OH footprinting, visualized by difference maps of the individual subunits and the intact ribosome, revealed unreported differences with the solvent accessible surface of the 16 S and 23 S rRNA calculated from crystal structures (Figure 2(e) and (f); marked by arrows; Table 3). Figure 3(a) shows the nucleotides in 16 S rRNA that are predicted to be inaccessible to solvent upon subunit association according to the crystal structure (yellow spheres) and those observed to be inaccessible to ·OH (yellow and orange spheres). Nucleotides protected from ·OH cleavage but solvent-accessible in the crystal structure are found in helix 11 in the 5′

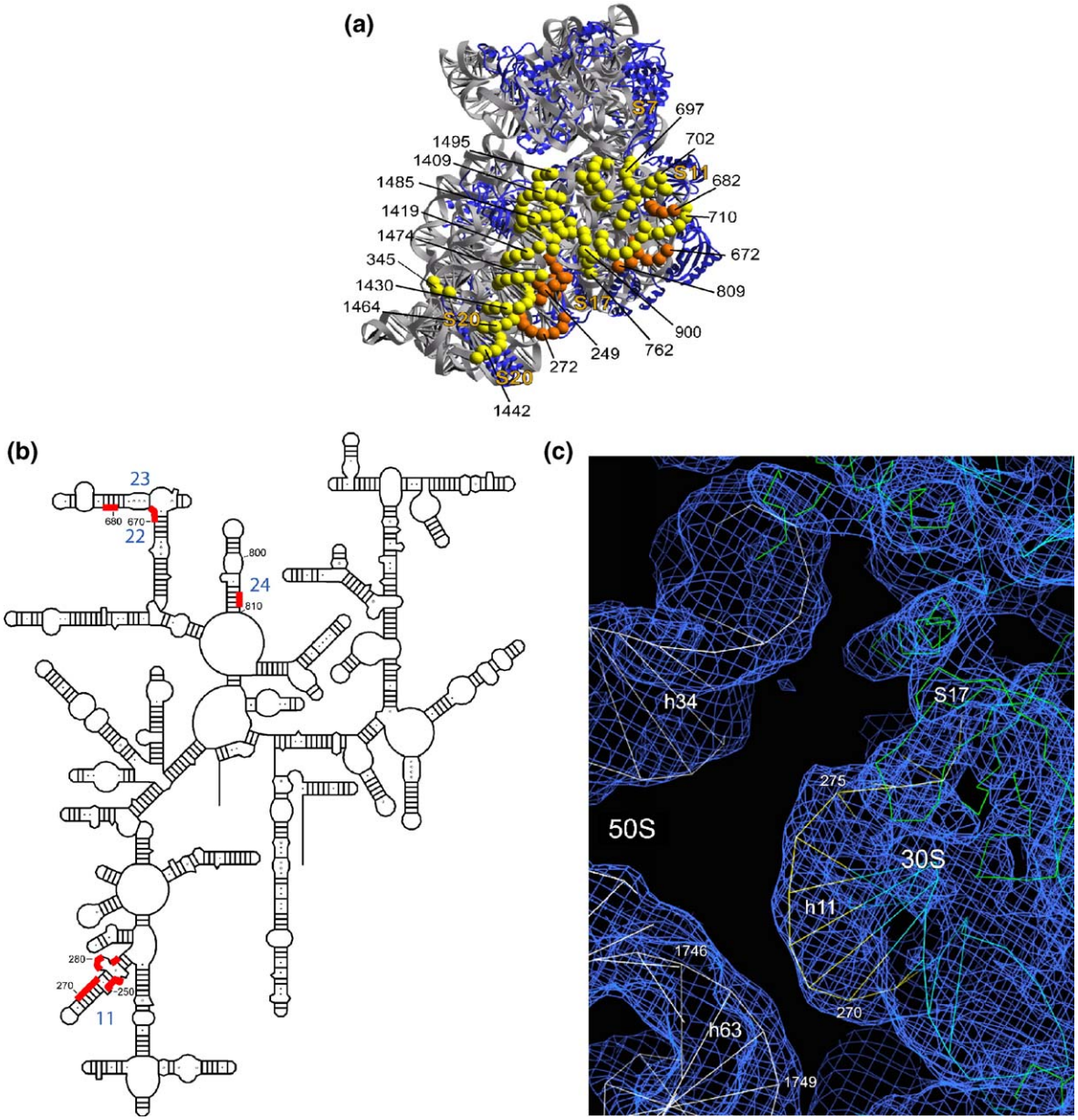

Figure 3. A structural summary of the locations of nucleotides in 16 S rRNA protected from ·OH upon subunit association. (a) Interface view of the 30 S subunit showing protected nucleotides that are predicted to be inaccessible (yellow spheres) or accessible (orange spheres) by NACCESS solvent-accessibility calculations. Thus, the orange spheres represent additional nucleotides protected from ·OH probing in solution that are not in contact according to the crystal structure. Representative nucleotides in each region are labeled. (b) Secondary structure of *T. thermophilus* 16 S rRNA, showing the positions of nucleotides (red circles) in helices 11, 22, 23 and 24 that are protected from ·OH by subunit association, but predicted to be solvent-accessible by NACCESS. (c) Electron density map (F_o contoured at 3σ) of the 5.5 Å *T. thermophilus* 70 S ribosome crystal structure[1] showing close proximity of the hydroxyl radical-protected nucleotides in helix 11 (h11) of 16 S rRNA to helix 63 (h63) of 23 S rRNA.

domain and in helices 22, 23 and 24 in the central domain (Figure 3(a), orange spheres; Figure 3(b)). These ''extra'' protections are localized in two clusters at the bottom of the body near positions 249 and 272 (Figure 3(a) on the right side of the platform (near positions 672, 682, and 809; Figure 3 (a)) of the 30 S subunit.

According to the 70 S crystal structure both regions are close to the surface of the 50 S subunit, but are not in direct contact with it. These protections can be explained by small differences between the conformation of the ribosome near the subunit interface in the crystal lattice and in solution. For example, the region around 16 S rRNA positions 249 and 272 is very close to nucleotides 1746-1749 of helix 63 of 23 S rRNA (Figure 3(c)). Similarly, nucleotides 679 and 682 are near positions 1846–1847 in helix 68 of 23 S rRNA; and nucleotides 806–809 are close to protein L2. All of these 16 S rRNA nucleotides could become protected from ·OH by movements of a few Angstrom units between the subunits. Positions 670–672, on the other hand, are not near enough to the 50 S subunit for their protections to be explained in this way. A more likely explanation is that interaction between proteins L2 and S6 in solution perturbs the structure or orientation of S6, moving it into contact with nucleotides 670–672.

In 23 S rRNA, there are two regions (ca 1740–1750 and 2150–2000) where protection is observed, both in the Fe-EDTA and X-ray probing experiments, but subunit contact is not predicted by NACCESS (Figure 2(f); Table 4). In the crystal structure, the first of these two regions (1740–1750) is juxtaposed to one of the protected regions of 16 S rRNA (249–272) discussed in the preceding paragraph, providing further evidence for formation of an additional inter-subunit contact in solution (cf. Figure 3(c)). The second set of protections (2150–2000) is located in the L1 arm of 23 S rRNA, which faces the platform of the 30 S subunit. The L1 arm has been shown to exist in several conformations in X-ray and cryo-EM studies,[1,12,28,38] indicating that it is a highly mobile structural element of the 50 S subunit. Our data suggest that the solution probing and X-ray structures reflect two different conformations of the L1 arm, possibly influenced by contacts with the 30 S subunit at the neighboring bridge B7a.

Table 4. Decreased reactivities of nucleotides toward hydroxyl radicals generated from Fe(II)EDTA compared to X-ray

16 S rRNA	23 S rRNA
182–183	402–405, 409, 411
186–192	613, 620
249–252	1045, 1061–1062
273–274	1066–1067
278–281, 284	1082–1088, 1094–1095
343	1573–1574, 1577–1579
700–703	1582–1586, 1589–1597
706–707	1722–1740, 1743–1752
	1754–1756, 1758, 1773
	2111–2116
	2131–2134
	2209–2210
	2303–2310
	2319–2326
	2333–2334
	2340–2341, 2343–2344
	2368–2373, 2376
	2399–2410
	2472–2474

Subunit stoichiometry

Quantitative footprinting depends on a linear relationship between measured changes in reactivity with either ligand concentration or time. Quantitative nucleic acid footprinting with ·OH is well established. The extent of backbone cleavage of shorter RNA molecules is conventionally assessed by monitoring the relative concentrations of end-labeled fragments of nucleic acids. Indirect detection by primer extension as used in these studies enables quantitative analysis of the much longer rRNAs[31] but introduces additional variables to data processing and analysis. Thus, a stoichiometric titration was conducted to verify the required linear response of the detection method and that the subunit association reactions progress to completion under the conditions of our experiments.

Equilibrium titrations of activated 30 S and 50 S subunits were conducted at subunit concentrations that exceed the K_d value of the association reaction (Figure 4). Under these conditions, a linear increase in protection terminating at the equivalence point is expected. Inter-subunit protections were monitored by synchrotron footprinting using primer extension of either the 16 S or the 23 S rRNA. Individually and together, the individual-site isotherms determined for the subunit interface protections are well described as a stoichiometric titration with the expected 1:1 equivalence of the 30 S and 50 S subunits. With these control experiments in hand, we next proceeded to an analysis of the kinetics of subunit assembly by synchrotron footprinting.

Association kinetics

Representative kinetics progress curves for formation of each of eight different inter-subunit bridges are shown in Figure 5. The ·OH protections analyzed were assembled from the respective protected nucleotides in 16 S rRNA (left column) and 23 S rRNA (right column) belonging to each inter-subunit bridge (Figure 1).[1] The data obtained for replicate experiments were globally analyzed. All of the kinetics progress curves were adequately described by a single exponential with an observed rate constant of ~2 s^{-1}; in all but one case, both the 16 S rRNA and 23 S rRNA sides of the inter-subunit contacts were analyzed (Figure 6). No variation in rate is observed among the inter-subunit contacts that exceed the experimental error. An approximate second-order rate constant of 16×10^6 M^{-1} s^{-1} for the formation of 70 S ribosomes is derived from these

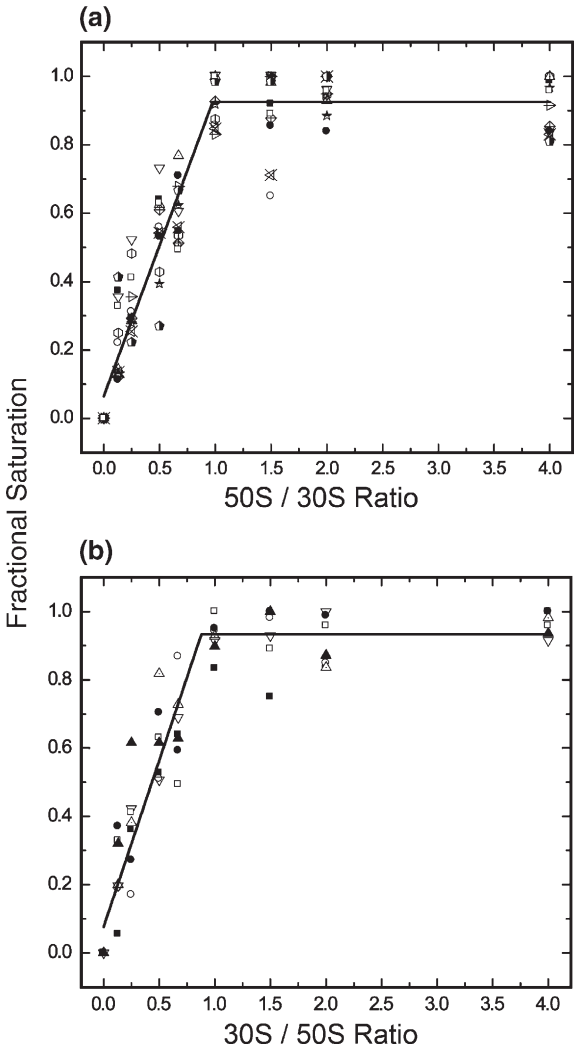

Figure 4. Stoichiometric titration of activated 30 S and 50 S ribosomal subunits followed by protection of inter-subunit contacts on (a) 16 S and (b) 23 S rRNA. The ·OH used for probing was generated by synchrotron X-ray radiolysis. The data shown include 11 regions of 16 S rRNA (●, 770–777; ◑, 782–785; ✦, 789–794; ⓘ, 799–802; ▷, 806–809; ⊠, 898–902; ▽, 1407–1416; ⊕, 1418–1422; △, 1425–1432; ○, 1440–1443, ■, 1471–1476) and seven regions of 23 S rRNA (▲, 1730–1735; ●, 1743–1752; □, 1765–1769; ▽, 1917–1926; ○, 1946–1952; △, 1959–1964; ■, 1986–1991). The continuous lines depict the best-fit intersection of two lines globally fit to the data. The equivalence points are 1.0 within experimental error for both graphs.

measurements obtained at subunit concentrations of 0.18 μM. This value is consistent with the previously reported rate constant of association of $16.2 \times 10^6\ M^{-1}\ s^{-1}$ at 20 °C and 6 mM Mg^{2+} [25] and with values determined in other studies under different experimental conditions.[32–37]

Discussion

The solvent accessibility of rRNA in ribosomal subunits and ribosomes was first studied using Fe(II)EDTA-generated ·OH as well as base-specific probes, yielding a comprehensive catalog of the features of rRNA that are involved in inter-subunit contacts.[14,15] Comparison of the reactivity of these probes in solution with the ribosome crystal structure[1] shows that most of the nucleotides protected by subunit association are on the contact surfaces of the inter-subunit bridges. This observation is supported by the quantitative comparison of the solvent accessible surface derived from ·OH probing and crystal structures presented in Figure 2. While confirming the overall agreement between the solution and crystal rRNA solvent accessibility, the differences shown in Figure 2 reveal subtleties to the subunit assembly reaction by summarizing the ·OH reactivity of thousands of nucleotides and highlighting the changes due to association. The clarity with which the inter-subunit contacts emerge from the noise of the experimental data is remarkable.

With a view toward monitoring the detailed structural dynamics of the ribosome, we have extended ·OH mapping for the study of the solution structure of ribosomes by quantifying the ·OH reactivity using radicals generated by synchrotron X-ray radiolysis as well Fe(II)EDTA. Difference between these methods of making radicals to be considered include (i) the time required to generate sufficient ·OH for footprinting is minutes for Fe(II)EDTA/ascorbate/H_2O_2 and milliseconds for radiolysis and (ii) radiolysis any of the 55 M of water molecules yields ·OH while the Fenton reaction is limited by the Fe(II)EDTA, peroxide and ascorbate concentrations. The identity of the 16 S rRNA ·OH reactivity difference maps obtained for the two methods of ·OH generation suggests that what matters is the ·OH, not how it is made (Figure 2(a) and (c)). This conclusion is supported by the overall agreement of the 23 S rRNA data (Figure 2(b) and (d)), validating the use of ·OH as a solution probe of the solvent accessible surface of the ribosome structure at nucleotide resolution.

However, the agreement is not complete for the 23 S rRNA; additional nucleotides protected from ·OH cleavage upon subunit association are visualized by X-ray radiolysis that are not seen by Fe-EDTA (Figure 2(d), asterisks). Inspection of the crystal structures yields no clear structural rationalization of these results. Since the sampling time of synchrotron radiolysis is hundreds of times shorter than the Fe(II)-EDTA protocol used, it might be envisioned that the X-ray probing reports a slow motion of the ribosome domains that is averaged out over time. However, this hypothetical motion would need to be triggered by the X-ray beam and synchronized for the ribosomes present in solution to be visualized by footprinting. How such an event would yield additional protections is difficult to fathom. Therefore, the origin of the X-ray radiolysis specific protections remains unclear at the present time. In the absence of a clear understanding of the methodological differences, we restrained our comparison of

solution and crystal solvent accessibility (Figure 3) to the protections common to both methods of $^{\bullet}OH$ generation.

Distinct differences are evident between the subunit assembly-dependent changes in the rRNA exposed surface areas predicted from solution probing with

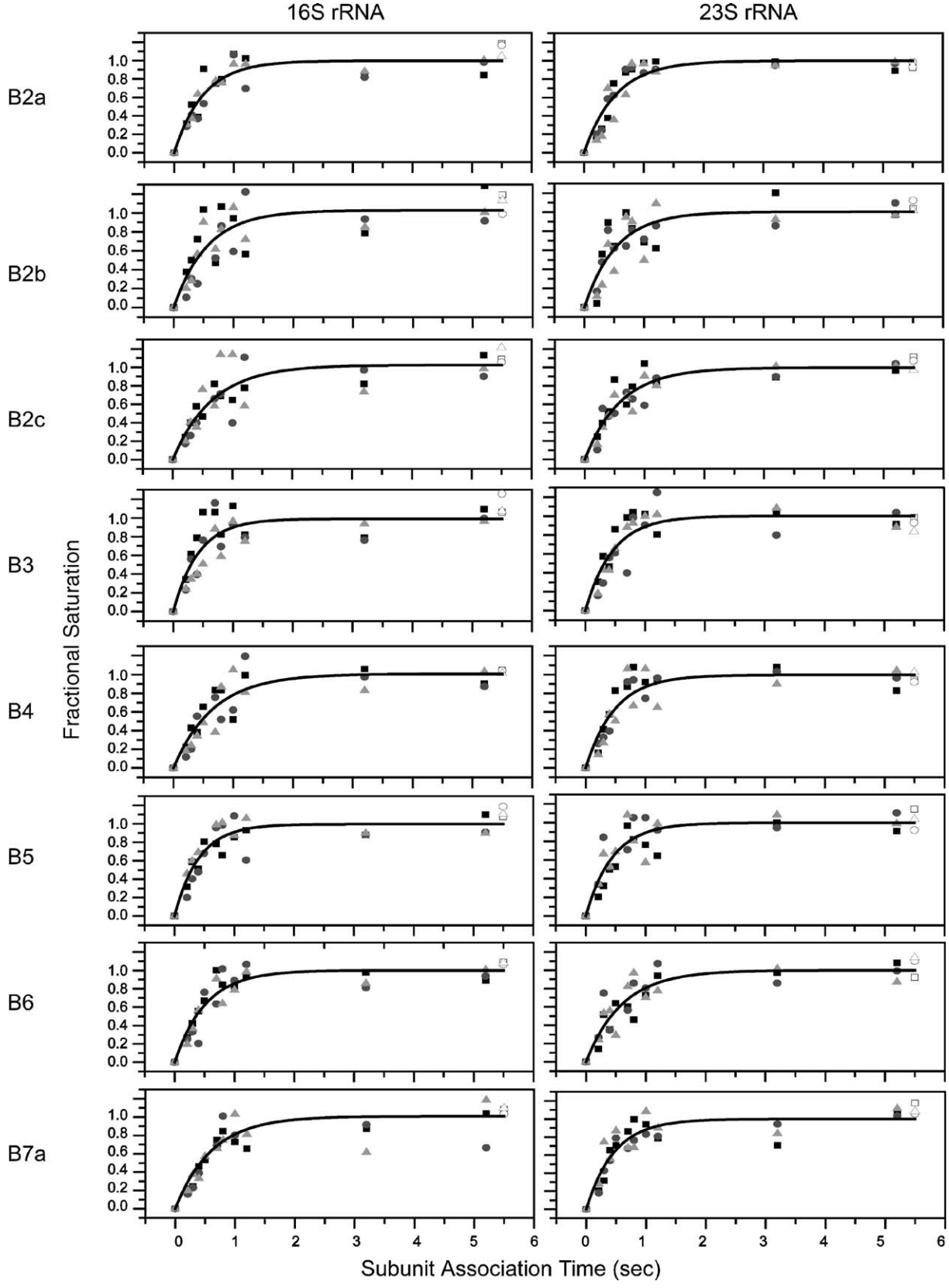

Figure 5 (*legend on opposite page*)

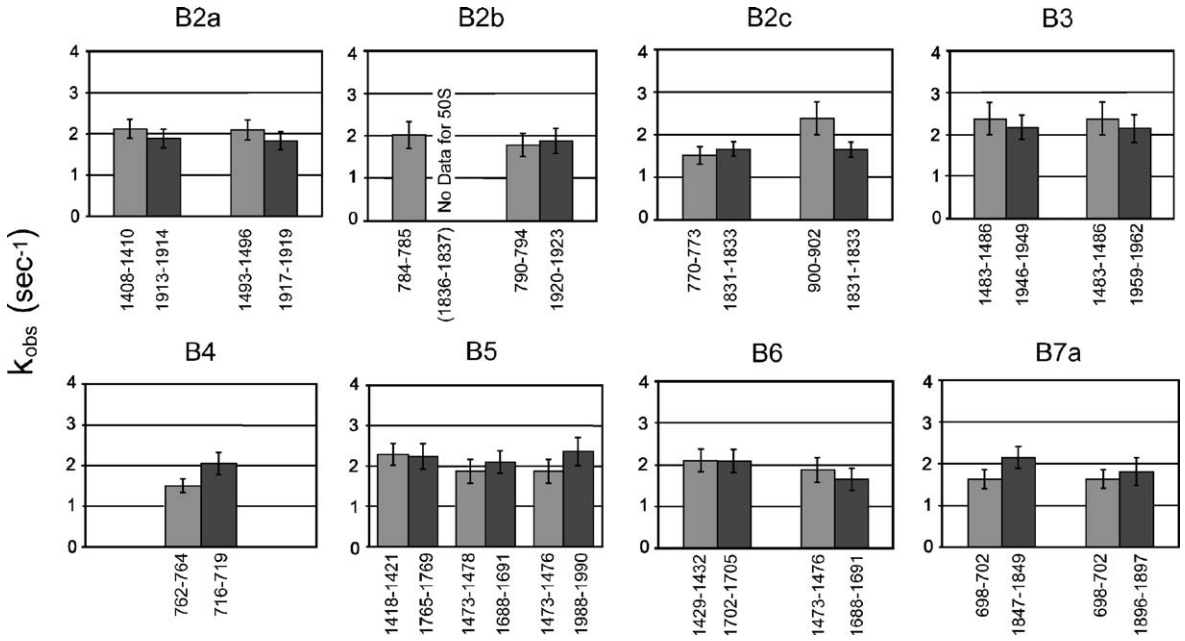

Figure 6. Histograms comparing the observed rates of ·OH protections determined for the 30 S (blue) and 50 S (red) RNA components of each of eight inter-subunit bridges (Figure 1) from kinetics progress curves such as those shown in Figure 5. Error bars represent the 95% joint confidence interval for the global analysis of the set of nucleotide protections that constitute the contact. (For interpretation of the references to colour in this figure legend, the reader is referred to the web version of this article.)

·OH calculated from the ribosome crystal structures despite the generally close agreement of these measures (Figure 3). Inspection of the recently determined crystal structures of two forms of the *E. coli* 70 S ribosome[38] shows surface accessibilities in these regions that are closely similar to those observed for the *T. thermophilus* 70 S crystal structure, ruling out the possibility that these discrepancies can be explained by phylogenetic differences.

When presented with these results we considered several hypotheses. The first hypothesis is that subunit association induces conformational changes that decrease the accessibility of the protected nucleotides. The second hypothesis is that subunit association blocks off solvent access to otherwise exposed surface. The extended exposure of much of the protected area in the 70 S ribosome crystal structure argues against both of these possibilities. That ·OH can be generated within pockets of trapped solvent by synchrotron radiation argues against the second hypothesis. The third hypothesis is that there are multiple states of subunit association, only one of which is represented by the 70 S crystal structures. Under our solution probing conditions, molecular interactions at the subunit interface may differ from those observed in the crystal lattices; additional inter-subunit contacts beyond those observed crystallographically may be possible. Precedent for this hypothesis is found in cryo-EM studies that reveal rearrangements of inter-subunit bridges between functional states of the 70 S ribosome.[12] Inspection of the electron density in the vicinity of the ''extra'' regions of subunit association-dependent ·OH protection (Figure 3(a)) suggests that the third hypothesis rationalizes most of these differences. The clearest examples are those for which both the 30 S and 50 S sides of additional ''contacts'' are evident by ·OH footprinting. As seen in Figure 3(c), helices 11 and 22–24 (30 S) and helices 63 and 68 as well as protein L2 (50 S) need only move closer by a few Ångstrom units to form a contact. A more indirect reasoning explains the extra ·OH protections involving nucleotides 670–672 of 16 S rRNA. In this case, interaction between ribosomal proteins L2 and S6 could perturb the structure or orientation of S6 in a way that brings it into contact with positions 670–672. The consistency of these structural correlations to the ·OH footprinting data suggests that such solution mapping will be a valuable tool in dissecting out the local changes in subunit structure that occur during catalytic cycling of the ribosome.

Figure 5. The time-evolution of the ·OH protection of nucleotides in (left) 16 S rRNA and (right) 23 S rRNA following formation of individual inter-subunit bridges during subunit association. The fractional saturation of groups of nucleotides in 16 S rRNA and 23 S rRNA, respectively, from bridges B2a (1408–1410, 1912–1194), B2b (790–794, 1920–1923), B2c (770–773, 1831–1833), B3 (1483–1486, 1946–1949), B4 (762–764, 716–719), B5 (1418–1421, 1765–1769), B6 (1473–1476, 1688–1691) and B7a (698–702, 1847–1849) were fit by non-linear least-squares to a single exponential decay. The individual nucleotides in each bridge are represented by different symbols. The open symbols at the far right of each plot indicate the ·OH reactivity of equilibrated associated subunits that provide an independent measure of the fully associated ribosome.

The kinetics progress curves determined for each of the eight inter-subunit bridges whose formation was quantified are identical, within experimental error (Figure 6). That the complementary 30 S and 50 S curves are likewise identical supports the validity of the data. All of these curves are adequately described by a single exponential consistent with a simple kinetic process (see below). The second-order rate constant of 16×10^6 M^{-1} s^{-1} calculated for these data is consistent with values determined by a variety of approaches that measure global properties.[25,33,39] Thus, the collection of individual local ·OH footprinting measures consistently reflect the ribosome's global association properties. Unimolecular processes significantly slower than bimolecular association are not seen in the ·OH footprinting progress curves. Hypothetical fast unimolecular processes are hidden by the rate-limiting bimolecular association (discussed below).

The time-resolved ·OH footprinting results are adequately fit by the simple reation scheme 30 S + 50 S ↔ 70 S that has been shown to describe subunit association.[25] The macroscopic picture presented by this collection of individual measures is that formation of the subunit interface occurs simultaneously. Microscopically, several mechanisms are possible for inter-subunit bridge formation. First, the bridges could form simultaneously in each ribosome in a rigid body interaction. The differences observed in the conformations of 23 S rRNA helices 38 and 69, for example, between the isolated subunits and the intact ribosome[1,3,28] strongly argues against this possibility. A more likely interpretation is that the formation of one or more bridges is rate limiting, followed by rapid formation of the remaining ones. Another possibility is that the bridges form sequentially, but in random order, masking any potential kinetic differences in their individual rates of formation. Our data do not distinguish among these alternative interpretations.

A recent study applied a novel quench-flow dimethyl sulfate (DMS) footprinting to the question of ribosome subunit assembly.[39] DMS is a base-specific probe that was used exclusively to monitor the reactivity of individual adenine bases in 16 S rRNA within the 30 S subunit. Since ·OH footprinting reports backbone accessibility, DMS and ·OH footprinting are complementary techniques. Of the eight adenine bases for which data are reported, only two (A702 and A1418) are involved in contacts with the 50 S subunit as seen in the 70 S crystal structure. Thus, the reactivity changes observed for the other six bases reported in the study were taken by these investigators to reflect association-dependent conformational changes.

Time points were acquired by these investigators as short as several milliseconds after mixing. Taking into account the difference in ribosome subunit concentrations present in the two assays, our interpretation of the time-evolution of the two inter-subunit bridges reported in common by the DMS and ·OH footprinting techniques, B7a and B5, is that they are comparable and reflect the overall bimolecular association reaction. However, the authors of this study interpret their data differently; they refer to their measures of the time-evolution of the A1418 and A702 as ''fast'' and ''slow'', respectively. In the absence of fits of their data to exponential decays it is unclear how these assignments were made. For example, the time-evolution of the A702 DMS protection appears coincident with their measurement of subunit association by light scattering.[39] While the fit of an exponential through the A1418 data is poor, it does yield a curve comparable to that obtained for A702. The lag seen in the A1418 and A1413 time-dependent data is unexplained and puzzling. The absence of normalization to a reaction endpoint and the aforementioned absence of data analysis cloud comparison of the ·OH and DMS footprinting results. However, if we take these results at face value an interesting connection with the ''encounter complex'' view of subunit assembly emerges.

The bases A702 and A1441 that are reported to exhibit ''slow'' rates appear to track with bimolecular association as noted above. Comparison of the conformation of A702 in the 70 S and 30 S crystal structures,[1,2,38] shows that it undergoes a substantial reorientation upon subunit association. Base A1441 lies in a phylogenetically variable region of helix 44 within the inter-subunit interface. Previous studies on chemical footprinting of ribosomal proteins on 16 S rRNA have shown that DMS and other base-specific chemical probes report ligand-induced conformational changes in the RNA, as well as ligand–RNA contacts, whereas ·OH tends to report mainly RNA–ligand contacts.[41,42] Thus, conformational change and subunit association are likely to influence the DMS reactivity of these bases. It is possible that the initial interface contacts involve mainly backbone interactions, followed by structural rearrangements that lead to additional interactions involving bases such as A702 and A1441. Other bases are reported to have ''fast'' reactivity with DMS; comparison of these progress curves with the light scattering measure of association suggests that they are faster than the subunit association reaction.[39] It will be interesting to see how well the observation of fast DMS reactivity changes stand up to more complete and precise data acquisition and analysis.

Ribosomal subunits association represents but a single step in the translation of mRNA. The catalytic cycling of peptide synthesis is controlled by an orchestrated series of conformational changes whose motions are being studied by a variety of techniques.[43] Can footprinting contribute to the emerging dialog about conformational change? As can be seen in our study and that by Hennelly *et al.*,[39] footprinting can report a full measure of local changes in the environment of the rRNA (e.g. Figure 2) allowing detailed structural events occurring in a large complex structure like the ribosome to be picked apart without losing sight of the whole. Since subunit assembly is a bimolecular reaction, its time course can be controlled *in vitro* by manipulation of the subunit concentrations. However, the

conformational changes that accompany peptide bond formation will be controlled by the rate of the catalytic cycling of this molecular machine. Thus, the use of time-resolved ·OH footprinting for the study of dynamic rearrangements occurring during protein synthesis will depend upon the accessible timescale. The time resolution of the present study was limited, since proteins also react with ·OH; the X-ray dose required to footprint the ribosome was much greater than that of free RNA. Technical innovations, including installation of a focusing mirror at NSLS beamline X-28C and development of alternative fast methods of ·OH generation[44] will allow large protein–nucleic acid complexes to be footprinted by ·OH at times limited only by the mechanics of the mixer. We therefore envision a role for footprinting along with crystallography, microscopy and single-molecule methods in deciphering the mechanism of translation.

Materials and Methods

Preparation of *E. coli* ribosomes and its subunits

Ribosomes were prepared from *E. coli* strain MRE 600 by the method of Staehelin & Maglott[45] with modifications as described[46] and stored at a concentration of 5–10 μM at −80 °C in 20 mM Tris–HCl (pH 7.5), 100 mM NH_4Cl, 10 mM $MgCl_2$, 6 mM β-mercaptoethanol (βME). The 30 S and 50 S subunits were isolated from dissociated ribosomes as described[14,15] and stored at –80 °C in 20 mM Tris–HCl (pH 7.5), 100 mM NH_4Cl, 10 mM $MgCl_2$, 6 mM βME.

Association of ribosomal subunits to form 70 S ribosomes

The 30 S subunits (50 μg in 25 μl) were activated in 50 mM potassium cacodylate (pH 7.5), 100 mM KCl and 20 mM $MgCl_2$ for 20 min at 42 °C as described.[14,15] For mapping experiments, 70 S ribosomes were prepared by associating activated 30 S and 50 S subunits at 37 °C for 20 min in 50 mM potassium cacodylate (pH 7.5), 100 mM KCl and 10 mM $MgCl_2$. The molar ratio of 30 S to 50 S subunits was 1:2 in the probing reaction for analysis of 16 S rRNA, and 2:1 for analysis of 23 S rRNA.[14,15]

Fe-EDTA (·OH) footprinting

Hydroxyl radical footprinting using Fe-EDTA-mediated Fenton chemistry was conducted in buffer containing 50 mM potassium cacodylate (pH 7.5), 100 mM KCl and 10 mM $MgCl_2$ Individual subunits or intact ribosomes (50 μg in 21 μl of buffer) were probed with 2 μl of a mixture of 50 mM $Fe(NH_4)_2(SO_4)_2{\cdot}6H_2O$ and 100 mM EDTA, and 2 μl of a mixture of 250 mM ascorbic acid and 2.5%(v/v) hydrogen peroxide.[47] The final concentrations of the subunits or ribosome were 2 μg/μl.

Synchrotron X-ray (·OH) footprinting

X-ray radiolytic footprinting was conducted using the white beam of station X-28C at the National Synchrotron Light Source (NSLS) at Brookhaven National Laboratory.[27,48,49] Dose-response measurements were conducted to determine the X-ray exposure necessary to achieve single-hit cleavage statistics for isolated subunits and complete ribosomes. Irradiation of 5 μg of subunits or ribosomes for 100 ms was typically required to achieve sufficient RNA cleavage comparable to that obtained with the optimized Fe(II)EDTA protocol. This exposure is long compared to those used to study pure RNA due to ·OH quenching by the protein component of ribosomes and ribosomal subunits. X-ray exposure times were adjusted in response to changes in the ring current and other operational parameters.

Exposure of samples to the X-ray beam can be accomplished in two ways at NSLS beamline X-28C. Static measurements were accomplished at room temperature using an electronic shutter[48] to control the X-ray exposure of 5 μg aliquots of ribosomes or ribosomal subunits in 10 μl of buffer suspended in a microfuge tube. The final concentrations of the subunits or ribosome were 0.5 μg/μl. The irradiated subunits were precipitated at –80 °C with 2.5 volumes of 95%(v/v) ethanol and 0.3 M sodium acetate (pH 6.5) for 10 min and pelleted by centrifugation at 15,000***g*** at 4 °C for 10 min. The titration experiments were carried out using activated 30 S and 50 S subunits in buffer containing 50 mM potassium cacodylate (pH 7.5), 100 mM KCl and 6 mM $MgCl_2$ at 4 °C.

Subunit association kinetics were studied using a modified KinTek quench-flow mixer equipped with a 15 μl X-ray exposure chamber.[27,48,49] Activated 30 S and 50 S subunits were associated at a 1:1 molar ratio (0.18 μM) in buffer containing 50 mM potassium cacodylate (pH 7.5), 100 mM KCl and 6 mM $MgCl_2$ at 4 °C. In these experiments, the subunits were mixed and allowed to associate for a defined period while protected from the X-ray beam. Following the programmed association time, the samples were then flowed past the X-ray beam such that their average exposure was 100 ms. The earliest data point collected was at 60 ms following the initiation of mixing. The irradiated samples were collected in microfuge tubes and flash-cooled to −80 °C immediately following sample elution.

Primer extension and gel electrophoresis

Products of ·OH were detected by primer extension as described.[47] Ribosomes were precipitated at –80 °C with 2.5 volumes of 95% ethanol and 0.3 M sodium acetate (pH 6.5) for 10 min, pelleted by centrifugation at 15,000***g*** at 4 °C for 10 min, resuspended (50 μg in 200 μl) in 0.3 M sodium acetate, 0.5%(w/v) SDS, 5 mM EDTA and extracted three times with an equal volume of buffer-saturated phenol at pH 7.9 and twice with chloroform. Glycogen (20 μg; Sigma) was used as a carrier to ensure quantitative recovery of the rRNA. Primer extension was carried out as described by Merryman & Noller.[47]

Gel quantification

Gels were imaged by exposure to a phosphor storage plate that was scanned and digitized using a PhosphorImager (Molecular Dynamics). The relative densities of the electrophoretic bands were determined from the digital images of gels as described.[50,51] Line profiles of 30–50 bands of each lane were determined using the

''create line graph'' function in the program ImageQuant (Molecular Dynamics). These profiles were then fit to a series of Lorentzian curves using the Peak Fitting Module from Origin v.6.1 (Origin Lab). The peak heights, widths and areas were inspected visually for consistency with the primer extension gels.[40] The peak area obtained for each band density, after background correction, corresponds to the relative reactivity to hydroxyl radicals at that nucleotide position. All reported peak areas were reproduced in two to six independent experiments. Titration isotherms and kinetic progress curves were scaled to fractional saturation as described.[48] Titration data were fit to the intersection of two lines to determine the stoichiometry by the non-linear least-squares method using the software Origin v.6.1 (Origin Lab).[52] Kinetics progress curves were fit to a single exponential decay to determine the observed rate constant k_{obs} also using Origin v6.1.[27]

Calculation of solvent accessible surface

An all-atom model excluding hydrogen atoms was generated from the crystallographic backbone trace of the 70 S *T. thermophilus* ribosome.[1] The rRNA bases were fitted to ensure an optimal base-pairing scheme and adjusted to the 5.5 Å electron density maps and the atomic resolution structures of the 30 S and 50 S subunits.[1–3] All-atom structures of ribosomal proteins in the 30 S subunit were adopted from the atomic resolution structures of the 30 S subunit.[2] The individual proteins (S2, S3, S4, S5, S6, S7, S8, S9, S10, S11, S12, S13, S14, S15, S16, S17, S18, S19 and S20) were fit to the electron density maps as rigid bodies.

The proteins are all-atom structures of the ribosomal proteins in the 50 S subunit that were adopted from crystal structures of the isolated proteins from *T. thermophilus* (or their close homologs from other organisms when available) and fit to the electron density. The modeled 50 S ribosomal proteins (with their sources and PDB accession numbers) are L1 (*T. th.*, 1AD2), L2 (*H. ma.*, 1JJ2), L3 (*D. ra.*, 1NKW), L4 (*H. ma.*, 1JJ2), L5 (*T. th.*, 1MJI), L6 (*B. st.*, 1RL6), No L7/L12, L9 (*B. st.*, 1DIV), L10 (*H. ma.*, 1JJ2) L11 (*T. ma.*, 1MMS), L13 (*H. ma.*, 1JJ2), L14 (*B. st.*, 1WHI), L15 (*H. ma.*, 1JJ2), L16 (*H. ma.*, 1JJ2), L17 (*T. th.*, 1GD8), L18 (*H. ma.*, 1JJ2), L19 (*D. ra.*, 1NKW), L20 (*D. ra.*, 1NKW), L21 (*D. ra.*, 1NKW), L22 (*T. th.*, 1BXE), L23 (*H. ma.*, 1JJ2), L24 (*H. ma.* 1JJ2), where *T. th.* is *Thermus thermophilus, H. ma* is *Haloarcula marismortui, D. ra.* is *Deinococcus radiodurans,* and *B. st.* is *Bacillus stearothermophilus*. The proteins L25, L29, L30, L31, L32, L33, L34, L35 and L36 were not included in the all-atom model.

The surface-accessible areas of individual atoms of a vacant 70 S structure generated as described above were calculated using the program NACCESS, rolling a 1.4 Å radius sphere over the van der Waals surface of the structural model.[1] The sum of the accessible surface areas of C4′ and C5′ atoms was then calculated for each nucleotide.

Acknowledgements

This work was supported by grants from the National Institutes of General Medical Sciences (RO1-GM017129 and PO1-GM066275) and Biomedical Imaging and Bioengineering (P41-EB001979). The National Synchrotron Light Source at Brookhaven National Laboratory is supported by the Department of Energy, Division of Materials Sciences. We thank G. Dhavan, N. Komas, S. Gupta, M. Sullivan, J. Toomey and M. R. Chance for their support in acquiring the X-ray footprinting data at NSLS beamline X-28C. We thank A. Baucom and C. Gorringe for creating the molecular graphics Figures.

References

1. Yusupov, M. M., Yusupova, G. Zh., Baucom, A., Lieberman, K., Earnest, T. N., Cate, J. H. D. & Noller, H. F. (2001). Crystal structure of the ribosome at 5.5 Å resolution. *Science*, **292**, 883–896.
2. Wimberly, B. T., Brodersen, D. E., Clemons, W. M., Jr, Morgan-Warren, R., Carter, A. P., Vonrhein, C. *et al.* (2000). Structure of the 30S ribosomal subunit. *Nature*, **407**, 327–339.
3. Ban, N., Nissen, P., Hansen, J., Moore, P. B. & Steitz, T. A. (2000). The complete atomic structure of the large ribosomal subunit at 2.4 Å resolution. *Science*, **289**, 905–920.
4. Yusupova, G. Z., Yusupov, M. M., Cate, J. H. & Noller, H. F. (2001). The path of messenger RNA through the ribosome. *Cell*, **106**, 233–241.
5. Ramakrishnan, V. (2002). Ribosome structure and the mechanism of translation. *Cell*, **108**, 557–572.
6. Wilson, D. N. & Nierhaus, K. H. (2003). The ribosome through the looking glass. *Angew Chem. Int. Ed. Engl.* **42**, 3464–3486.
7. Moore, P. B. & Steitz, T. A. (2003). The structural basis of large ribosomal subunit fucntion. *Annu. Rev. Biochem.* **72**, 813–850.
8. Frank, J., Verschoor, A., Li, Y., Zhu, J., Lata, R. K., Radermacher, M. *et al.* (1995). A model of the translational apparatus based on a three-dimensional reconstruction of the *Escherichia coli* ribosome. *Biochem. Cell Biol.* **73**, 757–765.
9. Frank, J. (2003). Toward an understanding of the structural basis of translation. *Genome Biol.* **237**, 1–77.
10. Mears, J. A., Cannone, J. J., Stagg, S. M., Gutell, R. R., Agrawal, R. K. & Harvey, S. C. (2002). Modeling a minimal ribosome based on comparative sequence analysis. *J. Mol. Biol.* **321**, 215–234.
11. Cate, J. H., Yusupov, M. M., Yusupova, G. Z., Earnest, T. N. & Noller, H. F. (1999). X-ray crystal structures of 70S ribosome functional complexes. *Science*, **285**, 2095–2104.
12. Valle, M., Zavialov, A., Sengupta, J., Rawat, U., Ehrenberg, M. & Frank, J. (2003). Locking and unlocking of ribosomal motions. *Cell*, **114**, 123–134.
13. Pogozelski, W. K. & Tullius, T. D. (1998). Oxidative Strand Scission of Nucleic Acids: Routes Initiated by Hydrogen Abstraction from the Sugar Moeity. *Chem. Rev.* **98**, 1089–1107.
14. Merryman, C., Moazed, D., Daubresse, G. & Noller, H. F. (1999). Nucleotides in 23 S rRNA Protected by the Association of 30 S and 50 S Ribosomal Subunits. *J. Mol. Biol.* **285**, 107–113.
15. Merryman, C., Moazed, D., McWhirter, J. & Noller, H. F. (1999). Nucleotides in 16 S rRNA Protected by the Association of 30 S and 50 S Ribosomal Subunits. *J. Mol. Biol.* **285**, 97–105.

16. Santer, M. & Shane, S. (1977). Area of 16S ribonucleic acid at or near the interface between 30S and 50S ribosomes of Escherichia coli. *J. Bacteriol.* **130**, 900–910.
17. Chapman, N. M. & Noller, H. F. (1977). Protection of specific sites in 16 S RNA from chemical modification by association of 30 S and 50 S ribosomes. *J. Mol. Biol.* **109**, 131–149.
18. Herr, W. & Noller, H. F. (1978). Nucleotide sequences of accessible regions of 23S RNA in 50S ribosomal subunits. *Biochemistry*, **17**, 307–315.
19. Herr, W., Chapman, N. M. & Noller, H. F. (1979). Mechanism of ribosomal subunit association: discrimination of specific sites in 16 S RNA essential for association activity. *J. Mol. Biol.* **130**, 433–449.
20. Herr, W. & Noller, H. F. (1979). Protection of specific sites in 23 S and 5 S RNA from chemical modification by association of 30 S and 50 S ribosomes. *J. Mol. Biol.* **130**, 1–32.
21. Lata, K. R., Agrawal, R. K., Penczek, P., Grassucci, R., Zhu, J. & Frank, J. (1996). Three-dimensional reconstruction of the *Escherichia coli* 30 S ribosomal subunit in ice. *J. Mol. Biol.* **262**, 43–52.
22. Gabashvili, I. S., Agrawal, R. K., Spahn, C. M., Grassucci, R. A., Svergun, D. I., Frank, J. & Penczek, P. (2000). Solution structure of the E. coli 70S ribosome at 11.5 Å resolution. *Cell*, **100**, 537–549.
23. Spirin, A. S. (1974). Structural transformations of ribosomes (dissociation, unfolding and disassembly). *FEBS Letters*, **40**, S38–S47.
24. Noll, M., Hapke, B. & Noll, H. (1973). Structural dynamics of bacterial ribosomes: II. Preparation and characterization of ribosomes and subunits active in the translation of natural messenger RNA. *J. Mol. Biol.* **80**, 519–529.
25. Pande, C. & Wishnia, A. (1986). Pressure dependence of equilibria and kinetics of *Escherichia coli* ribosomal subunit association. *J. Biol. Chem.* **261**, 6272–6278.
26. Noll, M. & Noll, H. (1976). Structural dynamics of bacterial ribosomes. V. Magnesium-dependent dissociation of tight couples into subunits: measurements of dissociation constants and exchange rates. *J. Mol. Biol.* **105**, 111–130.
27. Sclavi, B., Woodson, S., Sullivan, M., Chance, M. & Brenowitz, M. (1998). Following the Folding of RNA with Time-Resolved Synchrotron X-Ray Footprinting. *Methods Enzymol.* **295**, 379–402.
28. Harms, J., Schluenzen, F., Zarivach, R., Bashan, A., Gat, S., Agmon, I. *et al.* (2001). High resolution structure of the large ribosomal subunit from a mesophilic eubacterium. *Cell*, **107**, 679–688.
29. Lee, B. & Richards, F. M. (1971). The interpretation of protein structures: estimation of static accessibility. *J. Mol. Biol.* **55**, 379–400.
30. Nguyenle, T. (2004). Solution structure and dynamics of the ribosome. PhD dissertation, University of California, Santa Cruz.
31. Adilakshmi, T., Ramaswamy, P. & Woodson, S. A. (2005). Protein-independent folding pathway of the 16 S rRNA 5′ domain. *J. Mol. Biol.* **351**, 508–519.
32. Wishnia, A., Boussert, A., Graffe, M., Dessen, P. H. & Grunberg-Manago, M. (1975). Kinetics of the reversible association of ribosomal subunits: stopped-flow studies of the rate law and of the effect of Mg2+. *J. Mol. Biol.* **93**, 499–515.
33. Gorisch, H., Goss, D. J. & Parkhurst, L. J. (1976). Kinetics of ribosome dissociation and subunit association studied in a light-scattering stopped-flow apparatus. *Biochemistry*, **15**, 5743–5753.
34. Chaires, J. B., Tai, M., Huang, C., Kegeles, G., Infante, A. A. & Wahba, A. J. (1977). Relaxation kinetics of *E. coli* ribosomes. *Biophys. Chem.* **7**, 179–188.
35. Wishnia, A. & Boussert, A. S. (1977). The non-specific role of Mg^{2+} in ribosomal subunit association: kinetics and equilibrium in the presence of other divalent metal ions. *J. Mol. Biol.* **116**, 577–591.
36. Chaires, J. B., Pande, C. & Wishnia, A. (1981). The effect of initiation factor IF-3 on *Escherichia coli* ribosomal subunit association kinetics. *J. Biol. Chem.* **256**, 6600–6607.
37. Infante, A. A., Demple, B. & Chaires, J. B. (1982). Analysis of the Escherichia coli ribosome-ribosomal subunit equilibrium using pressure-induced dissociation. *J. Biol. Chem.* **257**, 80–87.
38. Schuwirth, B. S., Borovinskaya, M. A., Hau, C. W., Zhang, W., Vila-Sanjurjo, A., Holton, J. M. & Cate, J. H. (2005). Structures of the bacterial ribosome at 3.5 Å resolution. *Science*, **310**, 827–834.
39. Hennelly, S. P., Antoun, A., Ehrenberg, M., Gualerzi, C. O., Knight, W., Lodmell, J. S. & Hill, W. E. (2005). A time-resolved investigation of ribosomal subunit association. *J. Mol. Biol.* **346**, 1243–1258.
40. Shadle, S. E., Allen, D. F., Guo, H., Pogozelski, W. K., Bashkin, J. S. & Tullius, T. D. (1997). Quantitative analysis of electrophoresis data: novel curve fitting methodology and its application to the determination of a protein-DNA binding constant. *Nucl. Acids Res.* **25**, 850–860.
41. Stern, S., Powers, T., Changchien, L. M. & Noller, H. F. (1989). RNA-protein interactions in 30S ribosomal subunits: folding and function of 16S rRNA. *Science*, **244**, 783–790.
42. Powers, T. & Noller, H. F. (1995). Hydroxyl radical footprinting of ribosomal proteins on 16S rRNA. *RNA*, **1**, 194–209.
43. Noller, H. F. (2005). RNA structure: reading the ribosome. *Science.* **309**, 1508–1514.
44. Shcherbakova, I., Mitra, S., Beer, R. & Brenowitz, M. (2006). Fast Fenton footprinting: a laboratory-based method for the time-resolved analysis of DNA, RNA and proteins. *Nucleic Acid Res.* **34**, e48.
45. Staehelin, T. & Maglott, D. (1971). Preparation of Escherichia coli ribosomal subunits active in polypeptide synthesis. *Methods Enzymol.* **20**, 449–455.
46. Moazed, D. & Noller, H. F. (1986). Transfer RNA Shields Specific Nucleotides in 16S Ribosomal RNA from Attack by Chemical Probes. *Cell*, **47**, 985–994.
47. Merryman, C. & Noller, H. F. (1998). Footprinting and modification-interference analysis of binding sites on RNA. In *RNA: Protein Interactions, a Practical Approach* (Smith, C., ed), pp. 237–253, Oxford University Press, Oxford.
48. Ralston, C. Y., Sclavi, B., Sullivan, M., Deras, M. L., Woodson, S. A., Chance, M. R. & Brenowitz, M. (2000). Time-Resolved Synchrotron X-Ray Footprinting and Its Application to RNA folding. *Methods Enzymol.* **317**, 353–368.
49. Brenowitz, M., Chance, M. R., Dhavan, G. & Takamoto, K. (2002). Probing the structural dynamics of nucleic acids by quantitative time-resolved and equilibrium hydroxyl radical ''footprinting''. *Curr. Opin. Struct. Biol.* **5**, 648–653.
50. Takamoto, K., He, Q., Morris, S., Chance, M. R. & Brenowitz, M. (2002). Monovalent cations mediate formation of native tertiary structure of the *Tetrahymena thermophila* ribozyme. *Nature Struct. Biol.* **12**, 928–933.

51. Pastor, N., Weinstein, H., Jamison, E. & Brenowitz, M. (2000). A Detailed Interpretation of OH Radical Footprints in a TBP-DNA Complex Reveals the Role of Dynamics in the Mechanism of Sequence-specific Binding. *J. Mol. Biol.* **304**, 55–68.

52. Rashidzadeh, H., Khrapunov, S., Chance, M. R. & Brenowitz, M. (2003). Solution structure and interdomain interactions of the Saccharomyces cerevisiae ''TATA binding protein'' (TBP) probed by radiolytic protein footprinting. *Biochemistry*, **42**, 3655–3665.

Edited by J. Doudna

(Received 24 January 2006; received in revised form 10 April 2006; accepted 12 April 2006)
Available online 2 May 2006